Light-Induced Dielectrophoretic Manipulation of DNA

Marco Hoeb,* Joachim O. Rädler,† Stefan Klein,‡ Martin Stutzmann,* and Martin S. Brandt*
*Walter Schottky Institut, Technische Universität München, Garching, Germany; †Department für Physik, Ludwig-Maximilians-Universität München, München, Germany; and ‡Institut für Photovoltaik, Forschungszentrum Jülich, Jülich, Germany

ABSTRACT Light-induced dielectrophoretic movement of polystyrene beads and λ-DNA is studied using thin films of amorphous hydrogenated silicon as local photoaddressable electrodes with a diameter of 4 μm. Positive (high-field seeking) dielectrophoretic movement is observed for both types of objects. The absence of strong negative (low-field seeking) dielectrophoresis of DNA at high frequencies is in agreement with the similarity of the dielectric constants of DNA and water, the real part of the dielectric function. The corresponding imaginary part of the dielectric function governed by the conductivity of DNA can be determined from a comparison of the frequency dependence of the dielectrophoretic drift velocity with the Clausius-Mossotti relation.

INTRODUCTION

For the detailed understanding of the physical properties of DNA and for the realization of a variety of novel devices such as an integrated lab-on-a-chip, the ability to stretch, orient or sort DNA molecules is a key prerequisite. In 1950, Pohl first used dielectrophoresis (DEP) to move neutral polarizable matter in a nonuniform electric field (1). Starting with Washizu et al. in 1990, numerous groups have demonstrated that DNA can aggregate on planar metallic electrodes (2–6) or insulating constrictions (7,8) via dielectrophoresis. However, in these experiments, the contact geometry is fixed by lithographic patterning of metal electrodes. In contrast, electrodes can also be generated exploiting the photoconductivity of semiconductor layers upon illumination. Such transient or virtual electrodes can be generated at will and have been used in combination with electrophoresis (9–11) and dielectrophoresis (12–14) to optically move and trap beads or cells. Here, we extend dielectrophoretic movement of objects to DNA polyelectrolytes using light-induced electrodes in films of hydrogenated amorphous silicon (a-Si:H) to define the motion of the biomolecules. In particular, we study the frequency dependence of the dielectrophoretic movement of DNA and compare it to the predictions of theory and the movement of polystyrene beads under identical conditions.

DIELECTROPHORESIS

An inhomogeneous electric field $\vec{E}$ exerts a force $\vec{F} = \vec{p} \cdot \nabla\vec{E}$ on an electric dipole $\vec{p}$. The field gradient pulls (both permanent and field-induced) dipoles toward regions of high or low electric field strength, depending on the frequency of the electric field. The time-averaged DEP force $\langle F(t)\rangle$ acting on a polarizable particle of radius r exposed to an alternating and inhomogeneous electric field $\vec{E}$ can be approximated in terms of dipole effects (15) by

$$\langle F(t)\rangle = 2\pi\varepsilon_m r^3 \mathrm{Re}[K(\omega)]\nabla\vec{E}^2, \quad (1)$$

where ω is the angular frequency of the applied electric field and $K(\omega)$ the dipolar Clausius-Mossotti factor, which incorporates the frequency-dependent dielectric properties of the observed object and its surrounding medium. The Clausius-Mossotti factor, which determines the sign of the DEP force, is given by

$$K(\omega) = \frac{\varepsilon_p^* - \varepsilon_m^*}{\varepsilon_p^* + 2\varepsilon_m^*}. \quad (2)$$

Here, ε_p^* and ε_m^* describe the complex permittivities of the particle and the medium, respectively. Because bulk and surface dipoles as well as solvent effects described by Maxwell-Wagner theory contribute to the overall polarization, the components of the general frequency-dependent complex permittivities ε_p^* are more complicated than for bulk material. In their usual description (16), the complex permittivities $\varepsilon^* = \varepsilon + i(\sigma/\omega)$ depend on the dielectric constant ε and the electrical conductivity σ of the respective material as well as on the angular frequency ω of the electric field, as the particle polarization is not instantaneous. For colloidal particles, the conductivity consists of two components: the surface conductivity $\sigma_p = \kappa_p/r$, where κ_p is the surface conductance and r the radius of the spheres, and the bulk conductivity, which to good accuracy can be assumed to vanish (17,18). At most, $K(\omega)$ can vary from 1 to −0.5. The particle is said to experience positive DEP when $K > 0$ (high-field seeker) and negative DEP when $K < 0$ (low-field seeker).

Moreover, the AC fields used in DEP help reducing electrochemical reactions at the electrodes (such as the electrolysis of water) and suppress unwanted electrophoretic contributions, since charged particles experiencing alternating fields merely

Submitted November 15, 2006, and accepted for publication March 29, 2007.

Address reprint requests to M. Hoeb, Tel.: 49-89-2891-2755; E-mail: hoeb@wsi.tum.de.

S. Klein's current address is Applied Films GmbH & Co. KG, Siemensstrasse 100, 63755 Alzenau, Germany.

Editor: David P. Millar.

0006-3495/07/08/1032/07 $2.00

doi: 10.1529/biophysj.106.101188

vibrate around an average position (16,19). Hence, usage of higher frequencies allows application of higher voltage amplitudes necessary to achieve fast particle manipulation.

MATERIALS AND METHODS

Experimental setup

To realize light-induced dielectrophoretic manipulation of DNA, the setup shown in Fig. 1 was used. The device consists of two electrodes with an aqueous solution of DNA or polystyrene beads sandwiched in between. The upper electrode, in the following called the semiconductor electrode, consists of a 1 mm thick glass substrate, a 70-nm thick untextured ZnO layer and a 1 μm thick layer of intrinsic hydrogenated amorphous silicon grown by plasma-enhanced chemical vapor deposition. The highly doped ZnO serves as a metallic, transparent back contact. The lower electrode, the counter electrode, has a metal layer consisting of a 25 Å thick Titanium adhesion layer followed by a 50 Å thick Platinum layer, formed via electron beam evaporation onto a 170 $\pm$ 10 μm thick microscope slide (Assistent, Sondheim, Germany). The semitransparent metallic layers permit observation of the labeled DNA or beads through the counter electrode (the loss of fluorescence intensity is $<$35%). The lateral conductivity of the metallic counter electrode was determined to be $2 \times 10^3(\Omega\text{cm})^{-1}$, which is considerably higher than the conductivity of the electrolyte or the amorphous silicon in the dark. The semiconductor electrodes were cut into pieces of 10 $\times$ 10 mm^2. The ZnO layer of the semiconductor electrode was electrically contacted from the side via silver paste. The counter electrodes were 24 $\times$ 40 mm in size and also electrically contacted with silver paste. A Teflon foil (Bohlender, Grünsfeld, Germany) of 120 μm thickness was used as a spacer, yielding a constant separation between both electrodes.

The dark conductivity of hydrogenated amorphous silicon is typically of the order of 10^{-12}–$10^{-10}(\Omega\text{cm})^{-1}$ (20), whereas the conductivity of the aqueous DNA solution was adjusted to $8 \times 10^{-7}(\Omega\text{cm})^{-1}$. If an alternating voltage (frequency $\nu = \omega/2\pi$ from 1 to 1000 kHz) is applied between the two electrodes without illumination, the major part of the voltage will drop across the a-Si:H layer. The electric field strength in the solution is therefore expected to be low and homogeneous. Under these conditions, polarizable particles should only vibrate.

Local illumination of the semiconductor electrode changes the situation. Generation of electron-hole pairs in the semiconducting layer increases the conductivity of the illuminated silicon layer by several orders of magnitude to $\sim 10^{-5}$–$10^{-4}(\Omega\text{cm})^{-1}$ (21). Thus, the resistance of the photoconductive layer in the point of illumination drops below the corresponding value of the electrolyte and the applied voltage now mainly drops across the solution. As shown in Fig. 1, the field strength in the solution rises and the field distribution becomes inhomogeneous, as required to generate dielectrophoretic forces.

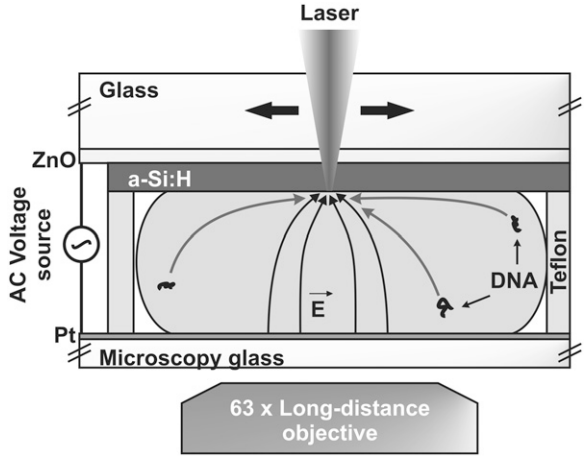

FIGURE 1 Schematic diagram of the setup used to observe light-induced dielectrophoretic movement of DNA.

The advantage of hydrogenated amorphous silicon as the photoconductive switch is the small ambipolar diffusion length of its charge carriers of $\sim$100 nm (22). Therefore, the size of the virtual electrode is largely determined by the size of the illumination. The size of the laser spot on the semiconductor electrode was $\sim$4 μm, as determined by measuring the full width ($\exp^{-2}$) of the intensity profile (not shown). For illumination, we used a 20 mW diode laser (Schäfter + Kirchhoff, Hamburg, Germany) emitting at a wavelength of 685 $\pm$ 5 nm into an optical fiber collimator. The laser beam was focused via a 100$\times$/NA 0.8 objective onto the semiconductor electrode through the glass substrate. A mechanical attenuator allowed sensitive and reproducible adjustment of the laser power over six orders of magnitude.

To monitor the dielectrophoretic movement, fluorescence microscopy was used. To this end, the setup shown in Fig. 1 was mounted on the sample stage of an epifluorescence microscope Axiovert 200 M Mat (Carl Zeiss, Oberkochen, Germany) equipped with a 63$\times$/NA 0.75 long-distance objective (working distance 2.2 mm). The micrographs were recorded with a Peltier-cooled 12 bit-CCD camera ORCA ER (Hamamatsu Photonics, Japan), which allows us to take images at a frequency of $(117\text{ ms})^{-1}$ per picture. For frame grabbing, the software OpenBox was used. The focal plane was typically set to be a few microns below the amorphous silicon layer inside the electrolyte solution. To block the light from the laser, a 600-nm short pass filter (Laser Components, Olching, Germany) was additionally introduced in front of the camera.

Samples

As the polarizable material, DNA and polystyrene beads were used in this study. Double-stranded 48.5 kbp DNA of the λ-phage (Sigma-Aldrich, St. Louis, MO) was marked with the intercalating fluorescent dye TOTO-1 (Molecular Probes, Eugene, Oregon) at an approximate dye/basepair ratio of one TOTO-molecule per 10 basepairs. For the stock solution, 50 μg DNA were dissolved in one milliliter of 10 mM sodium chloride solution. TOTO-1 dye was diluted to 10 mM in deionized water (dH_2O). Immediately before use, the DNA was stained by mixing the two solutions with deionized water (dH_2O) in a proportion of 9:2:1 (dH_2O:TOTO:DNA). The conductivity of the DNA-solution was determined via pH measurements to be $8 \times 10^{-7}(\Omega\text{cm})^{-1}$.

For the control experiments with polystyrene beads, we used two kinds of Fluospheres from Molecular Probes: negatively charged beads (via sulfate groups) with typical diameters of 2 μm and positively charged beads (via amine groups) with 1 μm diameter. Before use, the concentrated polystyrene solution (2% solids) was diluted with deionized water in a proportion of 1:60 (sphere solution:dH_2O) and vortexed to redisperse the microspheres. The conductivity of the latex solution is assumed to correspond to the conductivity of the dH_2O, which is $5.5 \times 10^{-8}(\Omega\text{cm})^{-1}$, as determined from the Millipore Synergy 185 deionization system. For the experiments, typically 3–4 μl of microsphere or DNA solution was used.

RESULTS AND DISCUSSION

Light-induced motion of polystyrene beads

As indicated in Fig. 1, an inhomogeneous electric field is generated via the focused laser light and we expect polarizable particles undergoing positive DEP to drift to regions of high field strength, i.e., underneath the illuminated part of the semiconductor electrode. In Fig. 2, we present a typical time series of fluorescence micrographs observed for negatively charged sulfate-modified polystyrene beads in the

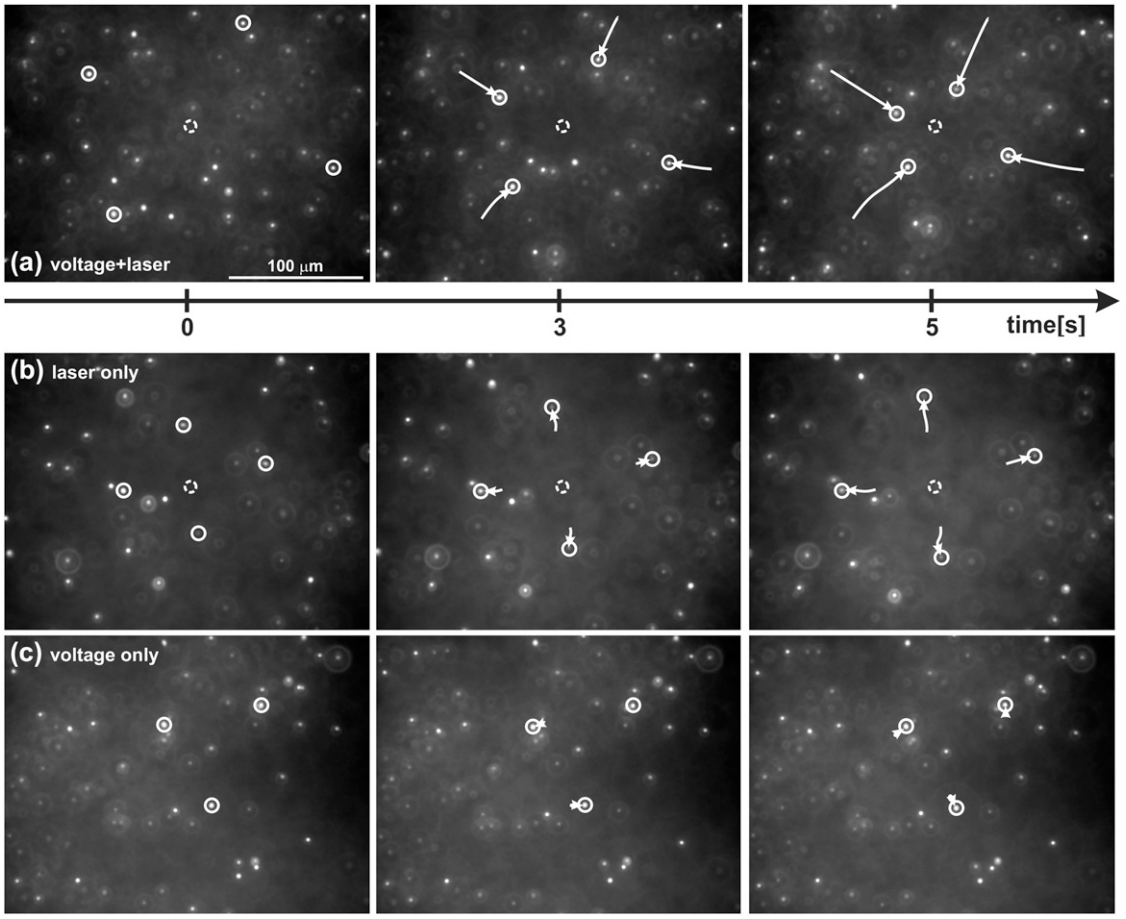

FIGURE 2 (*a*) Dielectrophoresis of negatively charged polystyrene beads under local illumination of the semiconductor electrode (1.1 mW) and application of an AC electric field (10 V peak-to-peak, $\nu = 100$ kHz). (*b*) Under illumination with the laser only, thermal effects lead to drift in the opposite direction. (*c*) Under application of the AC electric field only, purely Brownian motion is found. The arrows indicate the time trace of characteristic beads since $t = 0$. The dashed circle shows the position of the focused laser beam.

setup of Fig. 1 under different applied voltages and laser illumination conditions. The first row of Fig. 2 shows a sequence of fluorescence micrographs taken 0, 3, and 5 s after switching on the laser under application of an AC voltage of 10 V peak-to-peak at 100 kHz across the electrodes. The arrows indicate typical single particle trajectories approaching the focused laser beam in the center obtained from tracking the particle movement between each of the pictures taken at the repetition rate of $(117\ \text{ms})^{-1}$. The figure shows the time trace of particles, marked by the solid circles, relative to their starting point in the first picture at time $t = 0$. The dashed circle in the center represents the position of the laser spot. At a laser power of 1.1 mW, the spheres clearly move to the illuminated spot at the center.

The two other time series show reference measurements, without AC voltage applied in Fig. 2 *b* or without illumination in Fig. 2 *c*. When the semiconductor electrode is only illuminated with the laser, the particles slowly drift away from the center, as shown in Fig. 2 *b*. The laser increases the temperature in the vicinity of the illuminated spot and the resulting temperature gradient drives the objects away from the center, for example, by convection or thermophoresis (23). We further on call this ''thermo-induced drift''. Without the laser, the field distribution is uniform and the particles are expected to exhibit a motion, which is a superposition of a high frequency oscillation of the particle perpendicular to the focal plane, which cannot be resolved due to the frequencies higher than 1 kHz used, and a thermal motion of the beads. The observed particle movement (shown in Fig. 2 *c*) was affirmed to be Brownian by determining the velocity distribution. The distribution was fitted by a Gaussian profile and the resulting diffusion coefficient compared with the respective diffusion coefficient calculated from the Stokes-Einstein relation, which showed to be in good agreement. The reference measurements demonstrate that both illumination and alternating voltage are necessary to generate a dielectrophoretic attraction toward the illuminated spot.

To confirm that the movement is independent of the charge of the particles, we have repeated the experiment with positively charged, amine-modified microspheres, keeping all

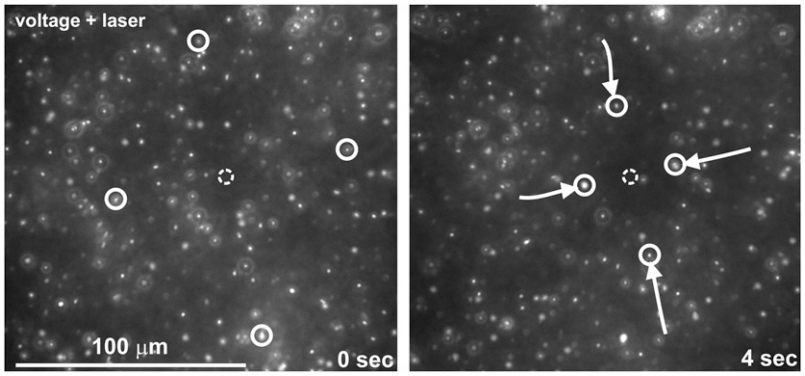

FIGURE 3 Dielectrophoresis of positively charged polystyrene beads under a 10 V peak-to-peak AC voltage at a frequency ν of 100 kHz and local illumination with a laser power of 1.1 mW, indicated by the dashed circle. As expected for dielectrophoresis, the direction of the force remains unchanged. The arrows again indicate the time trace of characteristic beads since $t = 0$.

other parameters constant. As seen from Fig. 3, simultaneous application of an AC voltage and local illumination of the semiconductor electrode leads to the same movement toward the illuminated spot, as expected for dielectrophoresis.

From the videos taken from these experiments, we have determined the momentary velocity of the beads moving to the laser spot to ~12 μm/s. Approaching the center, one should expect the velocity to increase with the gradient of the electric field. However, for the investigated distance range of 150–20 μm from the laser spot center we could not observe a noticeable change in the momentary velocity of the particles, which can already be seen in the time series in Fig. 2. This observation is in agreement with the results of Chiou et al., who tracked cells over a much shorter distance with a similar device and found an increase in the particle velocity approaching the illuminated spot only for distances <15 μm (14). This spatial dependence allows the definition of an average particle velocity depicted in Fig. 4 *a* for different AC frequencies and therefore a comparison of our experimental results with the theoretical prediction for the frequency dependence of the dielectrophoretic force, given by Eq. 2, for the polystyrene spheres.

The velocities of the polystyrene spheres $\overline{v_s}$ shown in Fig. 4 *a* are velocities averaged over four to six different microspheres. A positive average velocity indicates particles drifting toward the virtual electrode. Additionally, the average velocity of particles $\overline{v_{th}}$ determined with no AC voltage applied is indicated by the dashed line in Fig. 2 *b*. At low frequencies, the average drift velocity is ~12 μm/s. Above 100 kHz, the velocities decrease rapidly. Before a comparison with the Clausius-Mossotti model, we correct the acquired drift velocities for thermal gradient contributions determined and plot $\overline{v_s} - \overline{v_{th}}$ in Fig. 4 *b*.

The frequency dependence of the Clausius-Mossotti factor is included in Fig. 4 *b*. The velocity scale in Fig. 4 *b* is adjusted so that the low frequency limit of Re[$K(\nu)$] and the average particle velocity at low AC frequencies superimpose. The observed reduction of the velocity at high frequencies is in good agreement with the Clausius-Mossotti formula, predicting a zero crossing of the velocity at 650 kHz. As the absolute value of the thermo-induced drift velocity is small compared to both dielectrophoretic velocities at high and low frequencies, both positive and negative DEP can be realized in principle using photoinduced virtual electrodes necessary for a capture of a single particle and the construction of an optical trap (12).

Light-induced motion of DNA

Fig. 5 shows the corresponding experiments on light-induced dielectrophoresis of DNA. The same AC voltage of 10 V

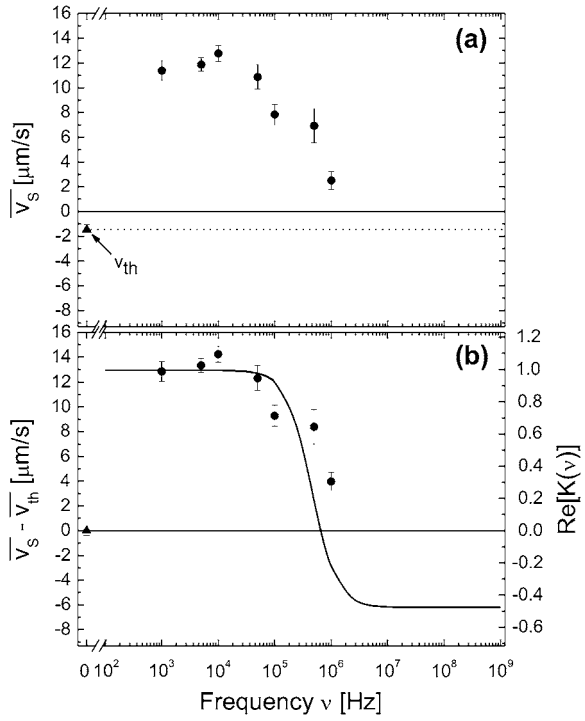

FIGURE 4 (*a*) Measured drift velocities for polystyrene beads undergoing dielectrophoresis as a function of frequency ν of the applied AC voltage with constant 10 V peak-to-peak amplitude averaged over four to six beads. The error bars indicate the standard deviation of the mean drift velocities. (*b*) Drift velocities of the polystyrene spheres corrected for thermo-induced drift and comparison to the Clausius-Mossotti factor. The calculation of Re[$K(\nu)$] was done with $\varepsilon_p = 2.55\ \varepsilon_0$ and $\varepsilon_m = 78.5\ \varepsilon_0$, where ε_0 is the permittivity of free space, $k_p = 2 \times 10^{-9}\ \Omega^{-1}$ and $r = 1\ \mu$m (17,18).

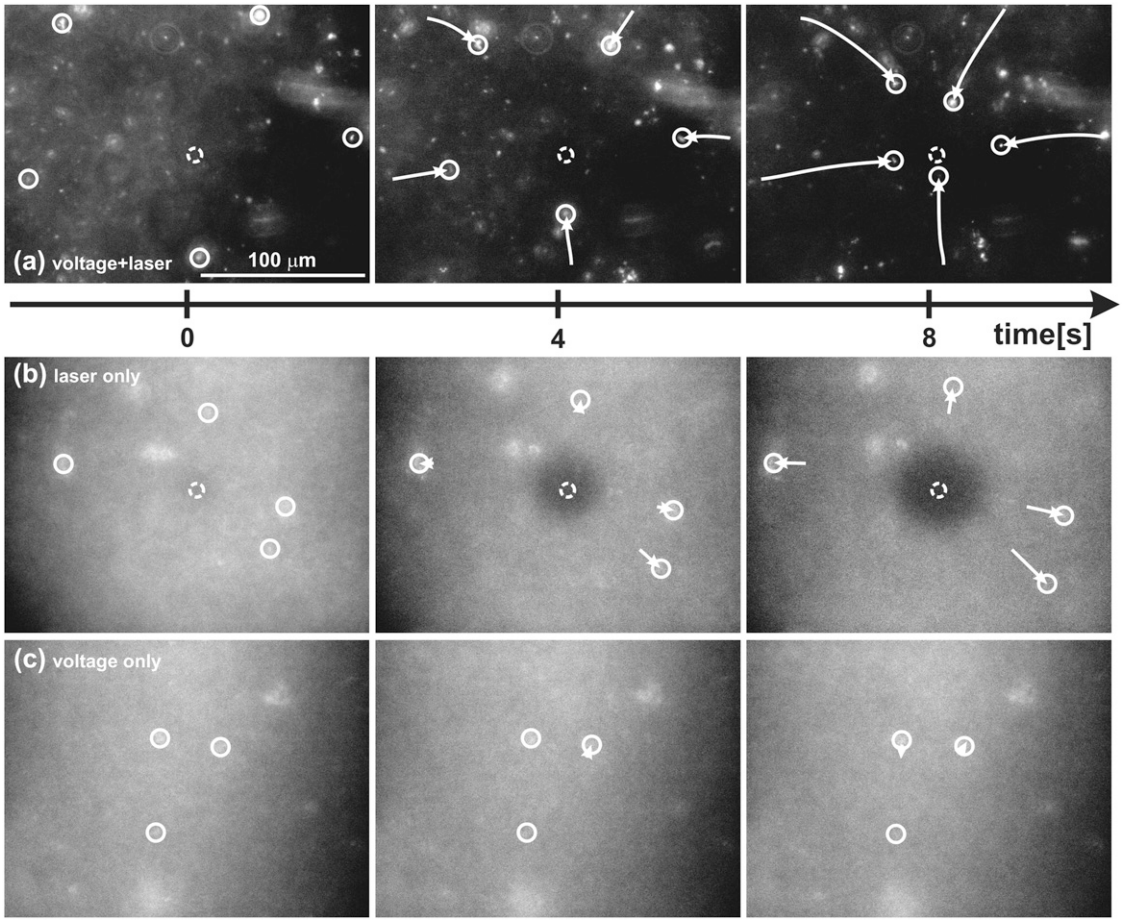

FIGURE 5 (*a*) Dielectrophoresis of DNA under local illumination of the semiconductor electrode (1.4 mW) and application of an AC electric field (10 V peak-to-peak, $\nu = 100$ kHz). (*b*) Under illumination with the laser only, thermo-induced with a drift in the opposite direction is observed. (*c*) Under application-induced of the AC electric field only, purely Brownian motion is found. The arrows again indicate the time trace of the DNA molecules since $t = 0$. The dashed circle shows the position of the focused laser beam. The contrast was digitally enhanced in each time series.

peak-to-peak at 100 kHz, but a slightly increased laser power of 1.4 mW, was used. Fig. 5 *a* shows that the DNA, stretched by the electric field gradient (not resolved), is again attracted to the highly photoconductive region, indicated by the dashed circle, with an average velocity of 7 μm/s. Fig. 5, *b* and *c*, summarizes the corresponding reference measurements. Fig. 5 *b* shows the effect of illumination only. A clear thermo-induced drift of single DNA molecules indicated by solid circles away from the area heated by the laser is observed. The origin of the lower contrast in Fig. 5, *b* and *c*, will be discussed below. The decrease of fluorescence intensity near the illuminated spot under these conditions is attributed to the effect of thermo-induced drift leading to a depletion of the heated central region, as suggested by Braun et al. (24,25) for thermophoresis. When the laser is switched off, the molecules drift back to the illuminated spot and the fluorescence recovers within a few minutes. Again, essentially only thermal motion of the molecules is observed (Fig. 5 *c*), if the AC voltage is applied only.

For the polystyrene beads and the DNA, no accumulation of the particles at the position of the focused laser beam was found under positive dielectrophoretic conditions at low frequencies. Instead, the particles approaching the laser spot were deflected to the counter electrode undergoing a convectionlike motion. This convection is not a dielectrophoretic effect, as the point of highest field gradient, and therefore the point all particles are attracted to, is the focused laser spot. Considering all forces contributing to the particle motion like sedimentation, thermo-induced, or laser-driven motion, the most probable explanation for the convection is the incompressibility of the electrolyte. The dielectrophoretically attracted objects drag electrolyte with them and thus lead to a flow, which converges at the point of laser illumination. Continuity demands a resulting flow perpendicular to the focal plane away from the a-Si:H electrode toward the counter electrode. This explains why particles are deflected out of the focal plane several micrometers before reaching the central laser spot on the amorphous silicon electrode.

This deflection of the particles out of the focal plane is also the reason for the better contrast of the first series of Fig. 5 *a* compared to the following time series, since these pictures were taken after a considerable time of dielectrophoretic

movement. The depletion-enhanced contrast can also be seen in time series Fig. 5 *b*. Here, the thermo-induced motion of the DNA molecules caused by the laser depletes the illuminated region, which leads to a time-dependent improvement of the molecule contrast.

Again, we compare the frequency-dependent average velocity $\overline{v_{\mathrm{DNA}}} - \overline{v_{\mathrm{th}}}$ of the polymers, determined as in the case of the polystyrene beads, with theory after taking into account thermo-induced effects (Fig. 6, *a* and *b*). Positive velocities again indicate molecules drifting to the center. Measured average drift velocities $\overline{v_{\mathrm{DNA}}}$ of the DNA together with the thermal effect of the laser only $\overline{v_{\mathrm{th}}}$ are shown in Fig. 6 *a*. Fig. 6 *b* illustrates the experimental drift velocity of the DNA molecules after correcting for the thermo-induced contribution together with the Clausius-Mossotti factor (again adjusted to superimpose at low frequencies).

First, one has to note that the apparent low-field seeking drift under illumination and AC voltage observed at high frequencies can be quantitatively attributed to thermo-induced drift. Since the real part of the dielectric function of DNA ε_{p} is essentially the same as ε_{m} of water (26), the Clausius-Mossotti factor approaches zero at high frequencies, so that only thermo-induced effects are to be expected in this frequency range, as indeed observed. These experiments can also be used to determine the surface conductivity σ_{p} of the polyelectrolyte. The imaginary part of the dielectric function of DNA (σ/ω) can then be obtained from a comparison of the frequency dependence of the average velocity with the Clausius-Mossotti factor, as performed in Fig. 6 *b*. Best agreement is found for $\sigma_{\mathrm{p}} = (3 \pm 2) \times 10^{-4}(\Omega\mathrm{cm})^{-1}$.

The conductivity of DNA is still subject to intense discussion with published results ranging from metallic to insulating behavior. Different experimental setups, used to determine the conductivity, seem to be responsible for these discrepancies. Several factors have been identified, which influence the charge propagation considerably, e.g., the sequence of bases in the DNA oligomers studied, dynamic disorder arising from structural fluctuations and environmental effects related to counterions in the aqueous solution (27). Also for λ-DNA investigated here, one can find literature values of the bulk conductivity of the polymer varying from 10^{-6}–10^{+3} $(\Omega\mathrm{cm})^{-1}$ (28–31). The advantage of our indirect determination is, that contact resistances or the number of molecules investigated in parallel do not have to be taken into account. The value of $\sigma_{\mathrm{p}} = 10^{-4}(\Omega\mathrm{cm})^{-1}$ obtained from Fig. 6 *b*, however, is likely to be dominated by charge transport through the ion cloud around the DNA molecules in the buffer solution, rather than to dry DNA (32). In fact, this value is similar to the insulating behavior observed by Braun et al. (30), where Na^{+} ions were also present in the experiments.

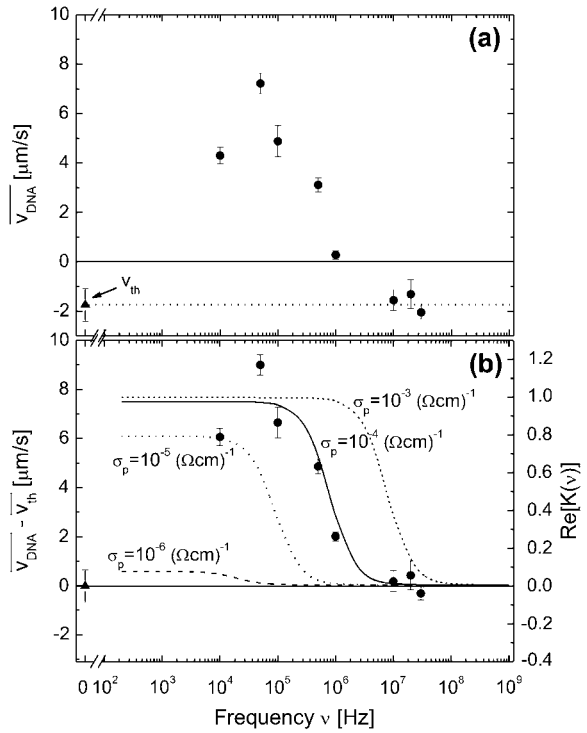

FIGURE 6 (*a*) Measured drift velocities for λ-DNA undergoing dielectrophoresis as a function of frequency ν of the applied AC voltage with constant 10 V peak-to-peak amplitude averaged over three to four molecules. The error bars again illustrate the standard deviation of the mean drift velocity. (*b*) Comparison of the Clausius-Mossotti factor and the average drift velocities for λ-DNA corrected for thermo-induced drift. The Clausius-Mossotti factor is shown for $\varepsilon_{\mathrm{m}} \approx \varepsilon_{\mathrm{p}} = 80\ \varepsilon_0$ and for various values of the surface conductivity σ_{p}.

CONCLUSION

We have demonstrated positive dielectrophoresis of differently charged polystyrene beads and of DNA in an optical manipulator using µm-sized local electrodes created by laser illumination of hydrogenated amorphous silicon as a means to photoswitch the electric field distribution. In particular, we have studied the influence of the applied frequency on the motion of the DNA and compared the results to theoretical predictions. The absence of negative dielectrophoresis at high frequencies is in agreement with the similarity of the dielectric constants ε_{p} and ε_{m} of DNA and water, respectively. The corresponding imaginary part of the dielectric function governed by the surface conductivity of the polyelectrolyte objects manipulated can be determined from the frequency dependence of the drift velocity, avoiding contact resistances and conformational difficulties. A comparison of the experimental results obtained for DNA with the theory of Clausius and Mossotti allows to estimate the electric conductivity of DNA in aqueous solution to $\sim 10^{-4}(\Omega\mathrm{cm})^{-1}$ for our experiments.

Collaboration with A. Härtl, S. T. B. Goennenwein, and S. Marx at early stages of this project is gratefully acknowledged.

We acknowledge financial support by Deutschen Forschungsgemeinschaft through grant No. SFB 563.

REFERENCES

1. Pohl, H. A. 1950. The motion and precipitation of suspensoids in divergent electric fields. *J. Appl. Phys.* 22:869–871.
2. Asbury, C. L., and G. v. d. Engh. 1998. Trapping of DNA in nonuniform oscillating electric fields. *Biophys. J.* 74:1024–1030.
3. Dewarrat, F., M. Calame, and C. Schönenberger. 2002. Orientation and positioning of DNA molecules with an electric field technique. *Single Molecules.* 3:189–193.
4. Washizu, M., and O. Kurosawa. 1990. Electrostatic manipulation of DNA in microfabricated structures. *IEEE Trans. Ind. Appl.* 26:1165–1172.
5. Washizu, M., O. Kurosawa, I. Arai, S. Suzuki, and N. Shimamoto. 1995. Applications of electrostatic stretch-and-positioning of DNA. *IEEE Trans. Ind. Appl.* 31:447–456.
6. Washizu, M., S. Suzuki, O. Kurosawa, T. Nishizaka, and T. Shinohara. 1994. Molecular dielectrophoresis of biopolymers. *IEEE Trans. Ind. Appl.* 30:835–843.
7. Chou, C. F., J. O. Tegenfeldt, O. Bakajin, S. S. Chan, and E. C. Cox. 2002. Electrodeless dielectrophoresis of single- and double-stranded DNA. *Biophys. J.* 83:2170–2179.
8. Chou, C. F., and F. Zenhausern. 2003. Electrodeless dielectrophoresis for micro total analysis systems. *IEEE Eng. Med. Biol. Mag.* 22:62–67.
9. Hayward, R. C., D. A. Saville, and I. A. Aksay. 2000. Electrophoretic assembly of colloidal crystals with optically tunable micropatterns. *Nature.* 404:56–58.
10. Ozkan, M., S. Bhatia, and S. C. Esener. 2002. Optical addressing of polymer beads in microdevices. *Sensors Mat.* 14:189–197.
11. Ozkan, M., C. S. Ozkan, O. Kibar, M. M. Wang, S. Bhatia, and S. C. Esener. 2001. Heterogeneous integration through electrokinetic migration. *Eng. Med. Biol. Mag.* 20:144–151.
12. Chiou, P. Y., A. T. Ohta, and M. C. Wu. 2005. Massively parallel manipulation of single cells and microparticles using optical images. *Nature.* 436:370–372.
13. Chiou, P. Y., Z. Chang, and M. Wu. 2003. A novel optoelectronic tweezer using light induced dielectrophoresis. *IEEE/LEOS International Conference on Optical MEMS.* 16:8–9.
14. Chiou, P. Y., A. T. Ohta, and M. C. Wu. 2004. Toward all optical lab-on-a-chip system: optical manipulation of both microfluid and microscopic particles. *Proc. SPIE Int. Soc. Opt. Eng.* 5514:73–81.
15. Gascoyne, P. R. C., and J. Vykoukal. 2002. Particle separation by dielectrophoresis. *Electrophoresis.* 23:1973–1983.
16. Jones, T. B. 1995. Electromechanics of Particles. Cambridge University Press, Cambridge, UK.
17. Morgan, H., M. P. Hughes, and N. G. Green. 1999. Separation of submicron bioparticles by dielectrophoresis. *Biophys. J.* 77:516–525.
18. Green, N. G., and H. Morgan. 1997. Dielectrophoretic separation of nano-particles. *J. Phys. D Appl. Phys.* 30:L41–L44.
19. Pohl, H. A. 1978. Dielectrophoresis. Cambridge University Press, Cambridge, UK.
20. Stutzmann, M. 1994. Amorphous semiconductors. *In* Handbook of Semiconductors. T. S. Moss and C. Hilsum, editors. Elsevier Science, Amsterdam, The Netherlands.
21. Vetterl, O., A. Groß, T. Jana, S. Ray, A. Lambertz, R. Carius, and F. Finger. 2002. Changes in electric and optical properties of intrinsic microcrystalline silicon upon variation of the structural composition. *J. Non-Cryst. Solids.* 299–302:772–777.
22. Schwarz, R., F. Wang, and M. Reissner. 1993. Fermi level dependence of the ambipolar diffusion length in amorphous silicon thin film transistors. *Appl. Phys. Lett.* 63:1083–1085.
23. Parola, A., and R. Piazza. 2004. Particle thermophoresis in liquids. *Eur. Phys. J. E.* 15:255–263.
24. Braun, D., and A. Libchaber. 2002. Trapping of DNA by thermophoretic depletion and convection. *Phys. Rev. Lett.* 89:1881031–1881034.
25. Duhr, S., S. Arduini, and D. Braun. 2004. Thermophoresis and DNA determined by microfluidic fluorescence. *Eur. Phys. J. E.* 15: 277–286.
26. Goswami, G., and N. Das Gupta. 1974. On the electric polarization of DNA. *Biopolymers.* 13:1549–1556.
27. Endres, R. G., D. L. Cox, and R. R. P. Singh. 2004. Colloquium: the quest for high-conductance DNA. *Rev. Mod. Phys.* 76:195–214.
28. De Pablo, P., F. Moreno-Herrero, J. Colchero, J. Gomez Herrero, P. Herrero, A. Baro, P. Ordejon, J. Soler, and E. Artacho. 2000. Absence of DC-conductivity in λ-DNA. *Phys. Rev. Lett.* 85:4992–4995.
29. Fink, H. W., and C. Schönenberger. 1999. Electrical conduction through DNA molecules. *Nature.* 398:407–410.
30. Braun, E., Y. Eichen, U. Sivan, and G. Ben-Yoseph. 1998. DNA-templated assembly and electrode attachment of a conducting silver wire. *Nature.* 39:775–778.
31. Zhang, Y., R. H. Austin, J. Kraeft, E. C. Cox, and N. P. Ong. 1998. Insulating behavior of λ-DNA on the micron scale. *Phys. Rev. Lett.* 89:1981021–1981024.
32. Kleine-Ostmann, T., C. Jördens, K. Baaske, T. Weimann, M. Hrabe de Angelis, and M. Koch. 2006. Conductivity of single-stranded and double-stranded deoxyribose nucleic acid under ambient conditions: the dominance of water. *Appl. Phys. Lett.* 88:1021021–1021023.